Study of In_2P/In_2P^- and InP_2/InP_2^- using negative ion zero electron kinetic energy spectroscopy

CAROLINE C. ARNOLD AND DANIEL M. NEUMARK[1]
Department of Chemistry, University of California, Berkeley, CA 94720, U.S.A.
and
Chemical Sciences Division, Lawrence Berkeley Laboratory, Berkeley, CA 94720, U.S.A.

Received June 15, 1994
Accepted June 27, 1994

This paper is dedicated to Dr. Gerhard Herzberg on the occasion of his 90th birthday

The zero electron kinetic energy (ZEKE) spectra of In_2P^- and InP_2^- are presented and compared to their previously obtained photoelectron spectra (PES) as well as ab initio calculations on analogous species. The threshold spectra, which give high-accuracy electron affinities of 2.400 ± 0.001 eV for In_2P and 1.617 ± 0.001 eV for InP_2, show well-resolved vibrational structure in the transitions from the ground anion states to the various neutral states. The ZEKE spectrum of In_2P^- exhibits a fairly extended, 47 cm^{-1} progression that we assign to the symmetric bend (ν_2) in the ground $^2B_1$ neutral state. There is also a 204 cm^{-1} progression that we assign to the symmetric stretch. The InP_2^- ZEKE spectrum shows transitions to two electronic states of the neutral. For the ground state, the symmetric stretch mode is the most active in the spectrum, whereas in the excited state, the symmetric bend mode is most active. The InP_2 ground-state symmetric stretch frequency is 190 cm^{-1}, and the excited-state symmetric bend frequency is 287 cm^{-1}. An anion ground-state frequency is determined to be 227 cm^{-1}. The term energy of the excited state is determined to be 1.280 ± 0.001 eV. Based on molecular orbital arguments, these frequencies suggest a $^2B_2$ ground InP_2 state, a $^2A_1$ first excited state, and a $^1A_1$ anion ground state.

Les spectres ZEKE (ionisation par électrons d'énergie cinétique nulle) de In_2P^- et de InP_2^- sont présentés et comparés aux spectres photoélectroniques (PES) obtenus antérieurement, ainsi qu'aux calculs *ab initio* effectués pour des molécules analogues. Les spectres seuils, qui donnent pour les affinités électroniques les valeurs de haute précision 2,400 ± 0,001 eV pour In_2P et 1,617 ± 0,001 eV pour InP_2, montrent des structures vibrationnelles bien résolues dans les transitions de l'état fondamental de l'anion vers les différents états de la molécule neutre. Le spectre ZEKE de In_2P^- présente une progression assez étendue de 47 cm^{-1} que nous attribuons à la flexion symétrique (ν_2) dans l'état neutre fondamental $^2B_1$. Il y a aussi une progression de 204 cm^{-1} que nous attribuons à l'élongation symétrique. Le spectre ZEKE de InP_2^- montre des transitions vers deux états électroniques de la molécule neutre. Pour l'état fondamental, le mode d'élongation symétrique est le plus actif dans le spectre, alors que pour l'état excité le mode de flexion symétrique est le plus actif. La fréquence d'élongation symétrique de l'état fondamental de InP_2 est 190 cm^{-1}, et celle de flexion symétrique de l'état excité est 287 cm^{-1}. La valeur déterminée pour l'énergie du terme de l'état excité est 1,280 ± 0,001 eV. Ces fréquences et des raisonnements sur les orbitales moléculaires suggèrent un état fondamental $^2B_2$ pour InP_2, un premier état excité $^2A_1$, et un état fondamental $^1A_1$ pour l'anion.

[Traduit par la rédaction]

Can. J. Phys. **72**, 1322 (1994)

1. Introduction

A considerable experimental and theoretical effort has been focused on the study of very small clusters in the hope that, by understanding the bonding in these species, insight toward the evolution of matter between the atomic and bulk scales will be gained. Clusters of pure semiconductor materials such as silicon have been of particular interest, owing to their potential technological importance. Mixed semiconductors are also important materials in circuit components as well as more exotic devices such as infrared light detectors and semiconductor injection lasers [1]. On the whole, spectroscopic investigations of pure semiconductor clusters have tended to lag behind the calculations, because of the dual requirements of size selectivity and spectral resolution in cluster spectroscopy experiments. For instance, only recently have ground- and excited-state frequencies been determined for Si_n ($n = 3, 4, 6, 7$) [2–5], whereas calculations have been ongoing for almost 10 years [6].

Mixed semiconductor clusters present the same experimental challenges and are also more of a challenge from a theoretical standpoint because of the wider range of structural permutations available in a binary system. Several calculations on small GaAs, InSb, and AlP clusters [7–11] have determined that multiple structural permutations possible for these species can in fact be close-lying in energy. In addition, each close-lying permutation may be congested with close-lying electronic states because of dangling bonds and, in some cases, open shells. The molecular geometries of small clusters are very different from bulk structures. Some of the compelling experimental questions regarding these small species, therefore, revolve around how the bonding in small clusters compares between clusters of similar atoms (i.e., the various III–V semiconductors) and how the bonding changes in clusters of different stoichiometries. The experimental work so far on mixed clusters leaves these questions largely unanswered. For example, although the electronic spectroscopy of several small GaAs and InP clusters has been studied by photoelectron and photodissociation spectroscopy, vibrational frequencies have only been measured for the diatomic and some of the triatomic species [12].

In this paper, we present zero electron kinetic energy (ZEKE) studies on In_2P^- and InP_2^- which, along with our previously obtained negative ion photoelectron spectra (PES),[2] were in part motivated by the experimental work on small indium phosphide clusters done by Mandich and co-workers. By using resonant

[1]Author to whom all correspondence should be addressed.

[2]C. Xu, E. de Beer, D.W. Arnold, C.C. Arnold, and D.M. Neumark. Manuscript in preparation.

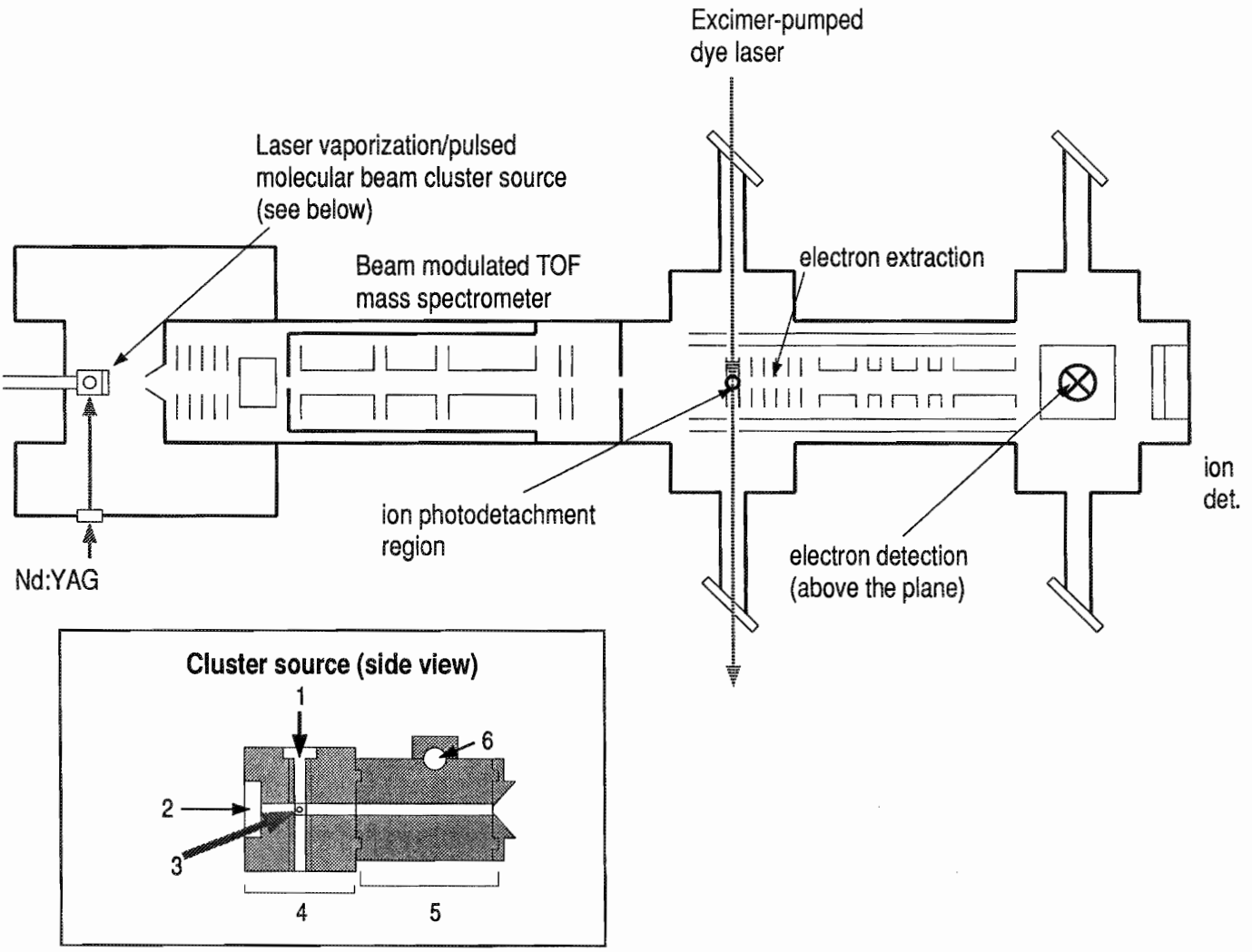

FIG. 1. Threshold photodetachment apparatus. The inset shows a detail of the cluster source in which the InP rod translates and rotates in a slot (1) and is intersected by pulses from the molecular beam (2) and Nd:YAG laser (3) in a Vespel piece (4). The copper clustering channel (5) is cooled by a copper tube carrying $N_{2(l)}$ (6).

one- and two-color photodissociation spectroscopy, Mandich mapped out the absorption of several clusters between 0.84 and 1.84 eV [13]. One of the interesting findings of Mandich's studies was that the energy of the HOMO–LUMO gap (or, more accurately, the lowest-energy transition allowed from the ground state) for the clusters, both stoichiometric and nonstoichiometric, was very near the band gap of bulk InP, although the odd-numbered clusters in these studies exhibited stronger absorption at lower energies. The PES studies of $In_xP_y^-$ mentioned above were complementary to Mandich's experiments; the clusters we investigated were in general smaller than those studied by Mandich, and more of the neutral states were accessed in our studies, but we observed size-dependent electronic structural trends similar to those revealed by Mandich. The only other work to date on small InP clusters is the infrared matrix isolation study by Weltner that yielded the InP diatomic frequency and the ν_3 mode for In_2P [12].

Both the work of Mandich and our PES data yielded some electronic structure for several mass-determined InP clusters, but no vibrational structure was resolved. The types of infrared or electronic absorption experiments that could determine vibrational frequencies are in general complicated by the presence of multiple species generated by most cluster sources. On the other hand, negative ion ZEKE spectroscopy is particularly well suited toward small cluster study, as it combines both mass selection and spectral resolution as high as 2–3 cm^{-1} (compared with 60–100 cm^{-1} for anion PES). Thus far, we have applied this technique toward the investigation of C_5^- [14], C_6^- [15], and Si_n^- (n = 2, 3, and 4) [4, 5] and have been able to resolve the low-frequency modes and closely spaced sequence band structure characteristic of these species.

The negative ion ZEKE spectra of In_2P^- and InP_2^- presented below show a rich electronic and vibrational structure that was unresolved in the PES, yielding detailed information on both the anion and neutral species. The In_2P^- ZEKE spectrum shows transitions to vibrational levels in at least two modes of the ground state of the neutral. The InP_2^- spectrum exhibits transitions to two electronic states of the neutral: the ground state and a low-lying excited state. The ZEKE spectra are compared with the corresponding PES,[2] as well with the calculations on the analogous In_xSb_y and Ga_xAs_y triatomics by Balasubramanian [7] and the $GaAs_2/GaAs_2^-$ anion calculations by Meier [9]. To aid in our analysis of InP_2, we have also performed our own ab initio calculations for frequencies and geometries at the MP2

level using an effective core potential basis set. The interesting frequency trends predicted for the two lowest-lying states of InP_2 are borne out well in our spectra. While we have not performed any frequency calculations for In_2P, the vibrational structure observed in the In_2P^- spectrum is consistent with the calculated ground electronic states of Ga_2As and In_2Sb.

The ZEKE spectra strongly indicate that the anions and neutrals for both species have C_{2v} geometries. In the In_2P neutral ground state, the bonding between the phosphorus atom and the indium atoms is much stronger than the bonding between the indium atoms, which is at most very weak. The anion exhibits stronger bonding among all of the atoms. For the InP_2 neutral ground state, the bonding between the two phosphorus atoms appears to be a strong, double covalent bond, with single bonds connecting each phosphorus to the indium atom. This is in contrast to the first excited state, which has comparatively weakened P–P bonding and stronger In–P bonding. The bonding properties in the InP_2^- ground state appear to lie between the two neutral states. These observations can be explained with reference to the molecular orbitals for the valence electrons.

2. Experiment

The threshold photodetachment apparatus used in these studies is discussed in detail elsewhere [16] but will be described briefly here. Figure 1 shows a schematic diagram of the apparatus employed in these experiments. A beam of cold indium phosphide cluster anions is generated in a laser vaporization – pulsed-molecular beam source similar to that developed by Smalley and co-workers [17]. The surface of a rotating, translating rod of InP is vaporized using 2–4 mJ/pulse of the 2nd harmonic output of a Nd:YAG operated at 20 Hz repetition rate. The resulting plasma is entrained in a pulse of He carrier gas from the molecular beam into a clustering channel. The gas then expands into the source chamber, and those negative ions passing through a 2 mm skimmer are colinearly accelerated to 1 keV and mass-selected using time-of-flight. The cluster of interest is then selectively photodetached using a (pulsed) excimer-pumped tunable dye laser. Only the electrons detached with nearly zero kinetic energy in the anion beam frame are collected as a function of photon energy. This selective detection of threshold electrons, based on the techniques developed by Müller-Dethlefs et al. for photoionization of neutrals [18], gives an energy resolution of 3 cm^{-1}.

For both molecules, the spectra were first obtained using the cluster source configuration that produced the coldest Si_4^- spectrum [4]; a piezoelectric molecular beam valve was used in conjunction with a 0.2 in. long, 0.15 in. inner diameter clustering channel terminated with a 0.1 in. exit slit (1 in. = 2.54 cm). This generates clusters with a vibrational temperature of approximately 200 K (higher frequency modes generally are hotter, whereas lower frequency modes are usually more efficiently cooled). After obtaining spectra of ions generated with the piezoelectric valve source, portions of the spectra were retaken using a new source incorporating a liquid-nitrogen-cooled clustering channel. This $N_{2(\ell)}$-cooled source, shown in the inset of Fig. 1, comprised a Vespel piece attached to the pulsed valve and the copper clustering channel. Laser vaporization and molecular-beam entrainment occurs in the Vespel piece, which serves to thermally insulate the pulsed valve from the cold clustering channel. The clustering channel is 1.25 in. long with an inner bore of 0.10 in. A terminal exit slit on the clustering channel was also required for the most effective cooling in this source configuration; it is also made of copper, and has an inner diameter of 0.05 in. A 1/8 in. copper tube carrying liquid nitrogen is fastened directly to the outside of the channel. Even with the insulating Vespel piece, some cooling of the pulsed valve occurred. We found the General Valve solenoid-type molecular beam valve to be more reliable with this source configuration, as the valve plunger tip was less sensitive to temperature than the O-ring tip used in the piezoelectric valve. By retaking a portion of the Si_4^- spectrum, we determined that the use of the cooled clustering channel further enhanced cluster cooling to a vibrational temperature of approximately 100–130 K.

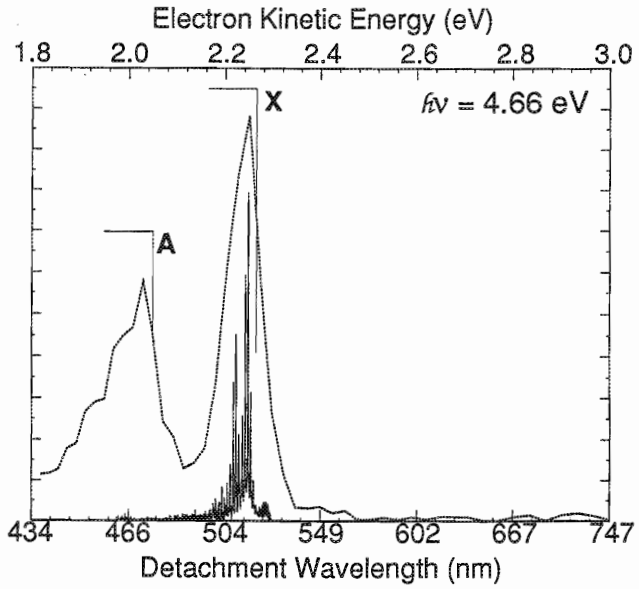

FIG. 2. ZEKE spectrum (solid line) superimposed onto the 266 nm (4.66 eV) photoelectron spectrum (broken line) of In_2P^-.

For In_2P^-, the photodetachment cross section was unusually large, and the signal was averaged for only 800 shots/point for the 200 K spectrum and 600 shots/point for the $N_{2(\ell)}$ portion of the spectrum. The dyes used for the spectrum were Coumarin 503, Coumarin 480, and Coumarin 450. For InP_2^-, the spectrum was signal averaged for 1500 shots/point for the 200 K spectrum and 800 shots/point for the $N_{2(\ell)}$ portion. The dyes used for InP_2^- were Rhodamine 800, LDS 722, LDS 698, Nile Blue 690, DCM, Rhodamine 640, Coumarin 440, Exalite 416, DPS, and QUI.

3. Results

3.1. In_2P^-

Figure 2 shows the ZEKE spectrum of In_2P^- (solid line) plotted vs. detachment wavelength. This is superimposed onto the previously obtained PES obtained with 4.66 eV photon energy[2] (broken line). For the energy scale of the PES, shown on the upper x axis, the electron kinetic energy (eKE) is given by

$$\text{eKE} = h\nu - EA - E_{\text{int}} \quad (1)$$

where $h\nu$ is the photon energy (4.66 eV), EA is the electron affinity of the neutral cluster, and E_{int} is the internal energy (vibrational, electronic, etc.) of the final neutral state. The PES shows two bands labeled **X** and **A**, which are 0.1–0.15 eV wide, respectively, and spaced 0.23 eV apart. These correspond to transitions to two electronic states of the In_2P: the ground state

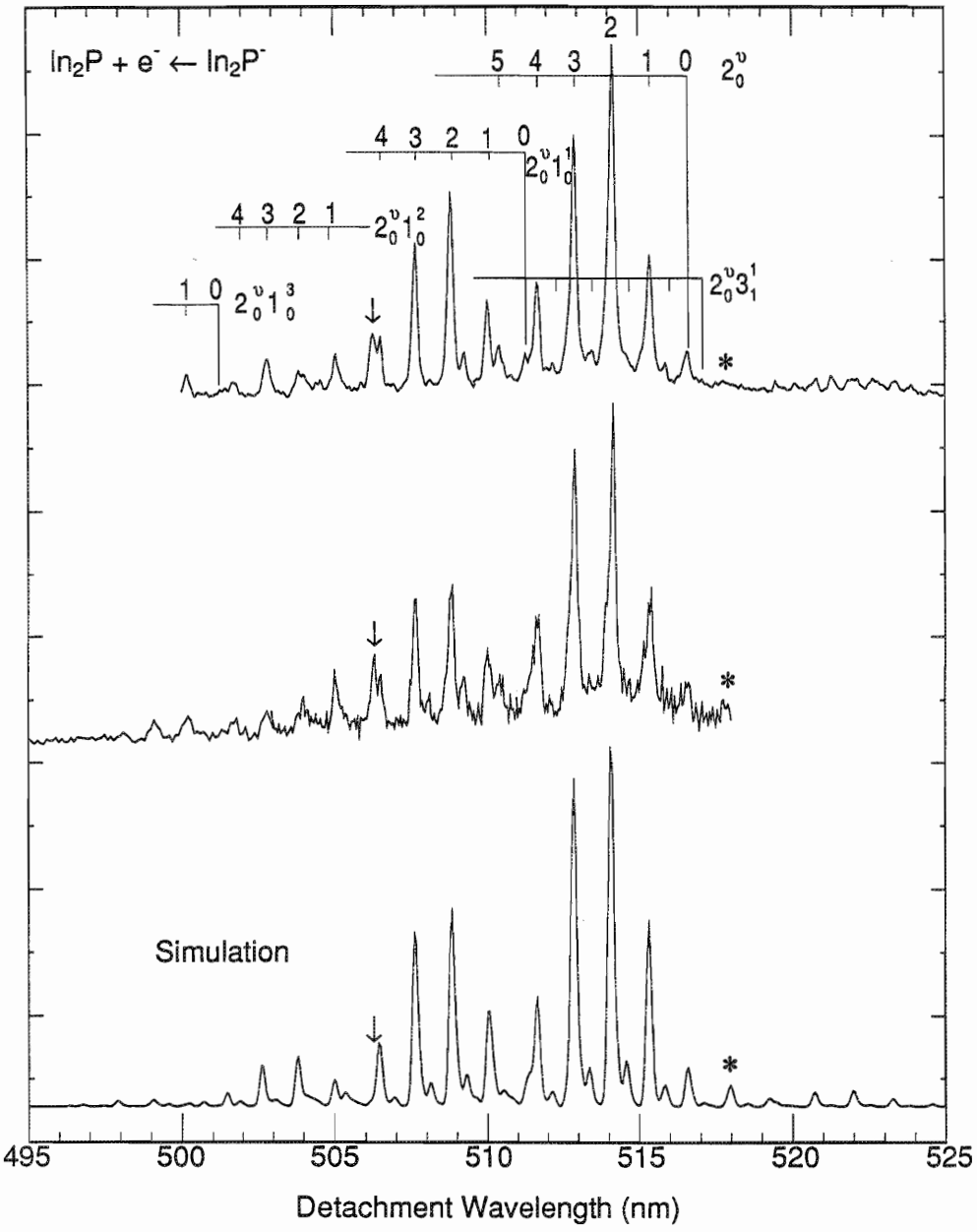

FIG. 3. ZEKE spectrum of In_2P^-. The upper trace shows data taken using ions generated with the liquid-nitrogen-cooled clustering channel, and the center trace with the piezoelectric valve source. The bottom trace is a spectral simulation (see text).

(**X**) and a low-lying state (**A**). The ZEKE spectrum in the energy region of band **X** shows extensive vibrational structure spaced by 47 cm^{-1}, which was unresolved in the PES. It is also apparent from the superimposed spectra that band **A** in the PES is absent in the ZEKE spectrum.

A detailed look at the ZEKE spectrum of band **X** is shown in Fig. 3, in which the upper trace was obtained from In_2P^- generated using the $N_{2(\ell)}$-cooled channel in cluster production, and the center trace was obtained using the room-temperature source. The peaks in both spectra are 8 cm^{-1} full width, half maximum (FWHM). The signal-to-noise ratio is clearly better in the upper trace, the baseline is better resolved between 510 and 515 nm, and several of the smaller peaks are less intense in the upper spectrum. All of these effects are consistent with colder ions in the upper spectrum and aid in identifying hot band transitions from vibrationally excited anions, such as the peak indicated with an asterisk, which is more intense in the center spectrum than in the upper spectrum.

The spectra show several vibrational progressions indicated by the combs in Fig. 3. The characteristic spacing in each progression is 47.0 ± 0.3 cm^{-1}. Peak 0 is the apparent origin of the most intense progression, labeled the 2_0^v progression, and is the lowest energy peak originating from the anion ground vibrational state. This yields an electron affinity of 2.400 ± 0.001 eV for In_2P. Three less intense progressions, labeled $2_0^v 1_0^n$ (n = 1–3), are found to the blue of the 2_0^v progression, and the origins of the four progressions are spaced by 204 ± 2 cm^{-1}. We are therefore observing vibrational progressions in two vibrational modes (ν_1 and ν_2) of *neutral* In_2P. The assignments of these modes will be discussed in detail in the next section, but for the purpose of presenting the data, the combs will serve as peak labels. There is also a peak found at 304 cm^{-1} from the most

intense 2_0^2 peak indicated with an arrow (↓). It is approximately at the right position to be the $2_0^0 1_0^2$ transition, but based on the patterns in the spectrum, it is anomalously intense. In the upper spectrum, there is a progression, labeled $2_0^v 3_1^1$, in which each peak is 27 cm^{-1} to the blue of a peak in the 2_0^v progression. The $2_0^v 3_1^1$ progression is better resolved than in the center spectrum, but the signal in the center spectrum seems to have more intensity overall. This structure appears to be a sequence band originating from vibrationally excited anions (with $v_3 = 1$) and will be discussed in detail below.

In the $N_{2(l)}$-cooled configuration, we also scanned the laser to lower photon energy and found the low-intensity hot bands between 519 and 525 nm (approx. 300 cm^{-1} to the red of the 2_0^v progression). This group of peaks has a characteristic spacing of around one-half the 47 cm^{-1} spacing of the 2_0^v progression. These features, along with the $2_0^v 3_1^1$ progression, appear to be the only progressions attributable to transitions from vibrationally excited anions.

Peak positions and relative energies for the ZEKE spectrum of In_2P^- are summarized in Table 1.

3.2. InP_2^-

The PES[2] of InP_2^- at a photon energy of 4.66 eV is shown in Fig. 4*c*. As with In_2P, this spectrum shows transitions to two electronic states of the neutral, labeled bands **X** and **A**. Figures 4*a* and 4*b* show the ZEKE spectra of InP_2^- plotted against detachment wavelength superimposed onto the vibrationally resolved PES obtained using two lower photon energies; the 355 nm spectrum of band **A** (the higher eKE region of the 355 nm spectrum was truncated to show only band **A**) shows a 280 cm^{-1} progression, and the 532 nm spectrum shows a partially resolved 190 cm^{-1} progression band **X**. More vibrational structure appears in the upper spectra because the resolution improves with lower eKE. In contrast to the In_2P^- spectrum, the two bands in the InP_2^- spectrum are 0.3 eV wide and spaced by approximately 1.28 eV. ZEKE spectra are observed for both bands, although in both cases the intensity profile of the structure in the ZEKE spectra does not appear to match the profiles of the bands observed in the PES. More detailed views of the ZEKE spectra of bands **X** and **A** are found in Figs. 5 and 6, respectively. Again, spectra obtained under the two source conditions are presented, with the "colder" data presented in Figs. 5*a* and 6*a* and the data acquired using the room temperature cluster source in Figs. 5*b* and 6*b*.

3.2.1. Band X

The ZEKE spectrum of band **X** shown in Fig. 5 is dominated by a 190.0 ± 0.2 cm^{-1} progression, with progression members indicated on the 2_0^v comb. Because of the extension of the progression, the origin transition will have very low intensity, and may in fact be obscured by the noise. The 2_0^0 peak corresponds to the lowest energy peak observed in this progression. We, therefore, take it as the origin, yielding an electron affinity for InP_2 of 1.617 ± 0.001 eV.

At higher photon energy, there is another, somewhat less intense progression with a characteristic spacing of 190 cm^{-1} indicated with the $1_0^1 2_0^4$ comb. In the center spectrum, the $1_0^0 2_0^v$ is the most intense member of the $1_0^1 2_0^v$ progression, peak 2_0^4 is the most intense of the 2_0^v progression, and the two peaks are spaced by 479 cm^{-1}, suggesting a 479 cm^{-1} frequency for a second neutral (ν_1) mode. This frequency is not entirely definitive from the spectrum, since the determination of the origin of the $1_0^1 2_0^v$ progression is made ambiguous by the sequence band progression, $2_0^v 3_1^1$, which overlaps somewhat with the $1_0^1 2_0^v$ progression. Each peak in the $2_0^v 3_1^1$ progression is approximately 78 cm^{-1} to the red of a 2_0^v transition, whereas the $1_0^1 2_0^v$ transitions are approximately 92 cm^{-1} to the red of the 2_0^{v+3} transitions. Although this difference in spacing allows us to discern unambiguously between the two progressions near the origin (where there are no $1_0^1 2_0^v$ transitions) and at higher photon energies (where the $1_0^1 2_0^v$ transitions will dominate), the first few members of the $1_0^1 2_0^v$ progression are small and overlap with the more intense part of the $2_0^v 3_1^1$ progression, giving rise to the possibility that the ν_1 frequency is actually (479 + 190) cm^{-1} or (479 − 190) cm^{-1}. However, the 479 cm^{-1} frequency is supported by our ab initio calculations presented below.

There is another progression, the 2_1^{v+1} progression, displaced 37 cm^{-1} to lower photon energy from the 2_0^v progression and assigned to a hot band progression originating from the anion $v_2 = 1$ level. The intensity profile of this progression differs somewhat from the others in that it peaks earlier. Although

TABLE 1. Peak positions and assignments for the In_2P^- ZEKE spectrum

Peak position (nm)	Energy from origin (cm^{-1})	Assignment
524.45−291		
523.85	−269	
523.36	−251	
522.63	−225	
521.97	−200	
521.28	−175	
520.77	−156	
520.09	−131	
519.43	−107	
517.76	−45	2_1^1
516.57	0	Origin; EA = 2.400 eV
515.85	27	$2_0^1 3_1^1$
515.34	46	2_0^1
514.15	91	2_0^1
513.46	118	$2_0^3 3_1^1$
512.90	139	2_0^3
512.15	168	$2_0^4 3_1^1$
511.65	187	2_0^4
511.26	201	1_0^1
510.39	235	2_0^5
510.00	250	$1_0^1 2_0^1$
509.25	279	2_0^6 , $1_0^1 2_0^2 3_1^1$
508.81	296	$1_0^1 2_0^2$
507.63	341	$1_0^1 2_0^3$
506.50	385	$1_0^1 2_0^4$
506.25	395	$2_0^2 3_0^2$
505. 03	443	$2_0^3 3_0^2$ or 3_0^2
504.48	464	
503.97	485	$1_0^3 2_0^2$
502.82	530	$1_0^2 2_0^3$
501.73	573	$1_0^2 2_0^4$
500.17	635	$1_0^3 2_0^1$

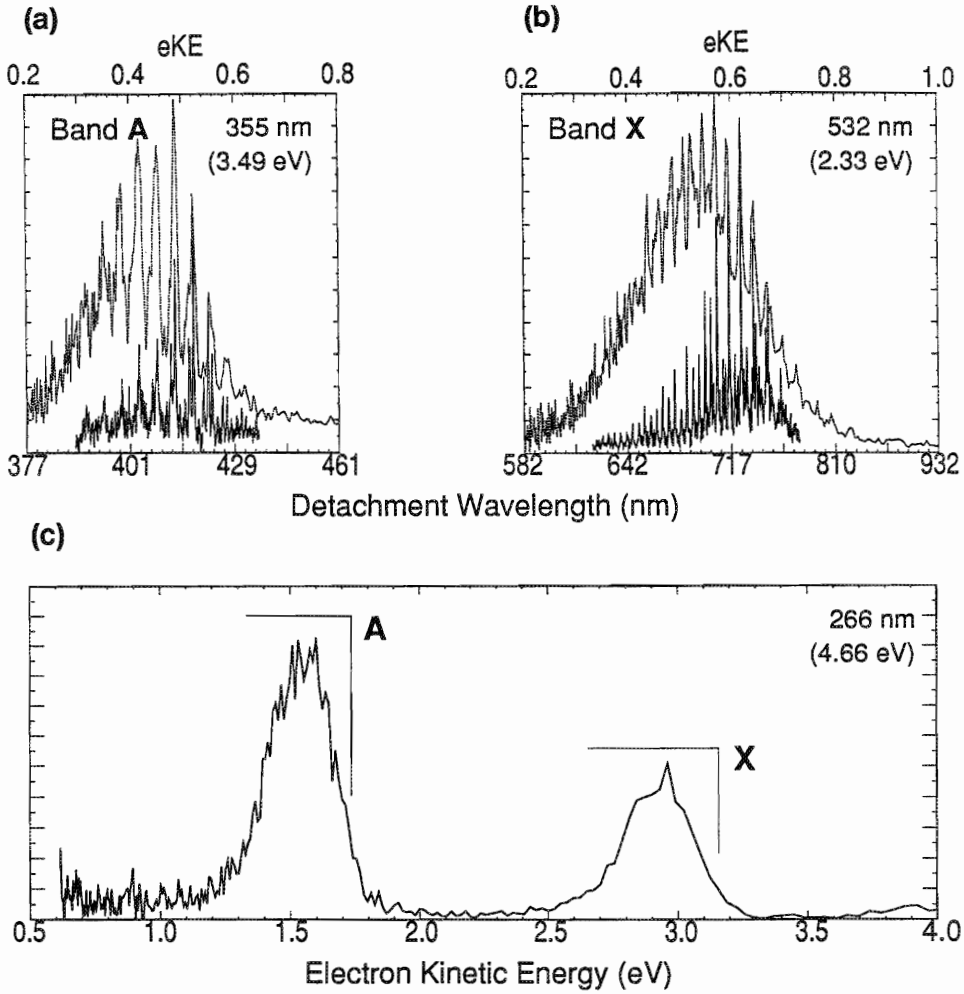

FIG. 4. (*a*) ZEKE spectrum of InP_2^-, band **A**, superimposed onto the 355 nm (3.49 eV) photoelectron spectrum. (*b*) ZEKE spectrum of InP_2^-, band **X**, superimposed onto the 532 nm (2.33 eV) photoelectron spectrum. (*c*) 266 nm (4.66 eV) photoelectron spectrum of InP_2^-.

the intensities of the 2_1^{v+1} progression are not uniformly less intense in the upper spectrum than in the center spectrum, the intensities in the center spectrum appear to be complicated by the overall congestion and lack of baseline between peaks. The 2_1^3, 2_1^4, and 2_1^5 transitions, however, are less intense in the upper spectrum. Another progression, labeled $1_0^1 2_1^{v+1}$ and displaced 37 cm^{-1} to the red of the $1_0^1 2_0^v$ progression, similarly peaks earlier than the $1_0^0 2_0^v$ progression.

Peak positions and relative energies for band **X** are summarized in Table 2.

3.2.2. *Band A*

Band **A** shown in Fig. 6 is dominated by a single progression with a 287 ± 1 cm^{-1} characteristic spacing indicated by the 2_0^v comb. The origin of this progression appears to be at 428.09 nm. The energy difference between the origins of bands **X** and **A** gives a term energy of 1.280 ± 0.001 eV for the excited state. Although there appears to be only one active mode in the spectrum, there are two additional progressions displaced approximately 60 and 75 cm^{-1} to the blue of the 2_0^v progression; these are labeled the 2_1^{v+1} and $2_0^v 3_1^1$ progressions, respectively, and have been assigned to transitions from singly excited anions. There are also several lower-intensity peaks apparently due to transitions from doubly excited anion vibrational levels. The main 2_0^v progression in the ZEKE spectrum (Fig. 6) not only fails to span the width of band **A** in the PES (Fig. 4) but the progression members broaden noticeably for $v > 2$.

Although the profile of the 2_0^v progression is clearly perturbed, it can still be seen that the relative intensities of peaks in the hot band 2_1^{v+1} progression compared to the 2_0^v peaks depend on v; for $v = 0$ and 1, the hot band intensities are greater than the corresponding transitions from the cold ions, whereas for $v = 2$, the hot band has less than half the intensity of the cold transition. In contrast, the intensity distribution in the $2_0^v 3_1^1$ progression approximately follows that of the 2_0^v progression.

A summary of the peak positions and relative energies for band **A** can be found in Table 3.

3.2.3. *Ab initio results*

Previous ab initio calculations [7, 9] on both $GaAs_2$ and $InSb_2$ predict a $^2B_2$ ground state and low-lying $^2A_1$ excited state, and a $^1A_1$ ground state for $GaAs_2^-$ (no calculations on $InSb_2^-$ have yet been published). Using the GAUSSIAN 92 software package [19], geometry and frequency calculations at the MP2 level using the LANL1DZ (Los Alamos National Laboratory double zeta) effec-

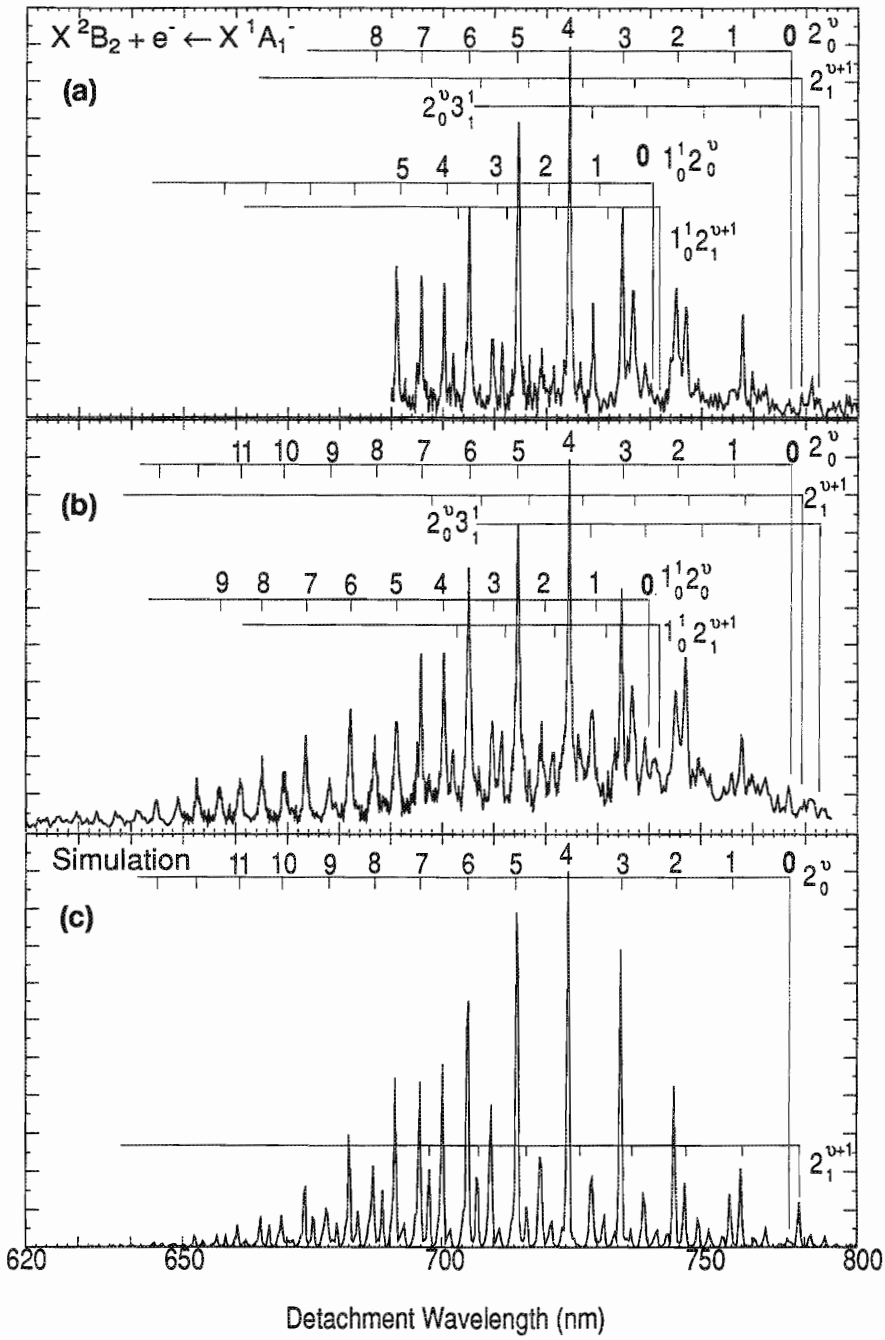

FIG. 5. ZEKE spectrum of InP_2^- to the neutral ground state (band **X**) obtained under (*a*) liquid-nitrogen-cooled source conditions and (*b*) ambient source conditions. (*c*) The Franck–Condon simulation.

tive core potential were performed for the two isovalent neutral states of InP_2 as well as the corresponding $^1A_1$ InP_2^- anion state.

The geometries, frequencies, and normal coordinates for these states in InP_2 as determined by the MP2 calculation are shown in Fig. 7. There are striking differences between the geometries and vibrational modes of the two neutral states. For instance, compared to the ground $^2B_2$ neutral state, the excited $^2A_1$ state has a shorter In—P bond by 0.34 Å (1 Å = 10^{-10} m) and a 0.3 Å longer P—P bond. The dramatic differences between the vibrational frequencies are also reflected in the disparate normal coordinates, as shown in Fig. 7. The term energy for the $^2A_1$ neutral state was calculated to be 1.139 eV. The $^1A_1$ anion ground state has both intermediate bonding relative to the two neutral states and, except for ν_1, intermediate vibrational frequencies.

Although our calculations are not as sophisticated as those performed by Balasubramanian [7] and Meier [9], we will see that the vibrational frequencies, geometry changes, and InP_2 excited-state energy are consistent with the two bands in the InP_2^- ZEKE spectrum. In assigning features in the ZEKE spectrum, it is therefore reasonable to assume that the InP_2 ground and excited states and the InP_2^- ground state are indeed

the $^2B_2$, $^2A_1$, and $^1A_1$ states, respectively, with properties close to those shown in Fig. 7. This assignment will be considered in more detail in Sect. 5.

4. Analysis

To understand the vibrational structure in the ZEKE spectra, it is useful to have a reasonable idea of the likely anion and neutral geometries. Without any a priori knowledge about these molecules, we are unable determine the point group of either based on the spectra alone. For In_2P^-/In_2P and InP_2^-/InP_2, there are four possible geometries that these species can assume: C_{2v}, $D_{\infty h}$, $C_{\infty v}$, and C_s. Balasubramanian's calculations on analogous neutrals [7] suggested that the $C_{\infty v}$ (i.e., Ga—As—As) and C_s structures are unstable with respect to rearrangement to C_{2v} structures. Our ab initio results on InP_2^- and InP_2 states presented in the previous section are on C_{2v} species, but as we made no attempt to establish the universal minimal anion and neutral geometries, we rely on the ab initio calculations by Meier et al. [9], who predicted that the linear structures for the analogous $GaAs_2^-$ and $GaAs_2$ were much higher in energy than the bent structures. Very acute bond angles (<50°) are predicted for the ground states of $InSb_2$, $GaAs_2$ and $GaAs_2^-$, and the low-lying excited states of $InSb_2$ and $GaAs_2$ are also predicted to be strongly bent [7]. If the predicted trends hold for InP_2, then one would expect the InP_2^- ZEKE spectrum to represent transitions between C_{2v} anion and neutral structures we have calculated.

The Ga_2As and In_2Sb ground states are predicted to have an obtuse geometries with bond angles of 109.5° and 104°, respectively [7], but no calculations on the anions analogous to In_2P^- have been performed. However, the progressions in the ZEKE spectrum are relatively short, indicating a fairly small change in geometry between anion and neutral. Thus, if neutral In_2P is an obtuse C_{2v} structure with a bond angle in the range of 100°–110°, then the anion most likely has an obtuse C_{2v} structure as well. On the other hand, the calculations predict low-lying linear ($D_{\infty h}$) excited states for both Ga_2As and In_2Sb, so we must consider the possibility that these are in fact the ground states and that we are observing transitions from linear or nearly linear In_2P^- and linear In_2P.

4.1. In_2P^-/In_2P

4.1.1. Band X vibrational structure and peak assignments

Given the above discussion, the geometries of both the neutral and anion can be inferred with reasonable certainty considering several points. First, the In_2P^- ZEKE spectrum exhibits a substantial amount of activation in two modes of the neutral, with the 47 cm^{-1} mode being more active than the 204 cm^{-1} mode. In electronic spectroscopy, one typically observes progressions only in totally symmetric vibrational modes. The presence of two active modes therefore argues against a linear ← linear transition, as this would show significant activation in the sole totally symmetric mode with possibly a small amount of activation in double quanta of the degenerate bend and (or) the antisymmetric stretch. Moreover, if the neutral were linear, spin-orbit splitting effects would be obvious in the spectra, since there is at least one unpaired electron in In_2P; no such effects are observed. From Balasubramanian's calculations [7], the lowest-lying linear state is a $^2\Pi_u$ state, but even if it were a $^2\Sigma$ state, the zero field splitting should be on the order of several hundred wave numbers (for In_2, the energy splitting between the components of the lowest-lying $^3\Sigma$ state was calculated to be on the order of 0.1 eV [20]). The overall appearance of the spectrum thus suggests a C_{2v} ground state for In_2P, consistent with the ground states predicted for isovalent Ga_2As and In_2Sb ground states. As mentioned above, this means that In_2P^- most likely has a C_{2v} geometry as well.

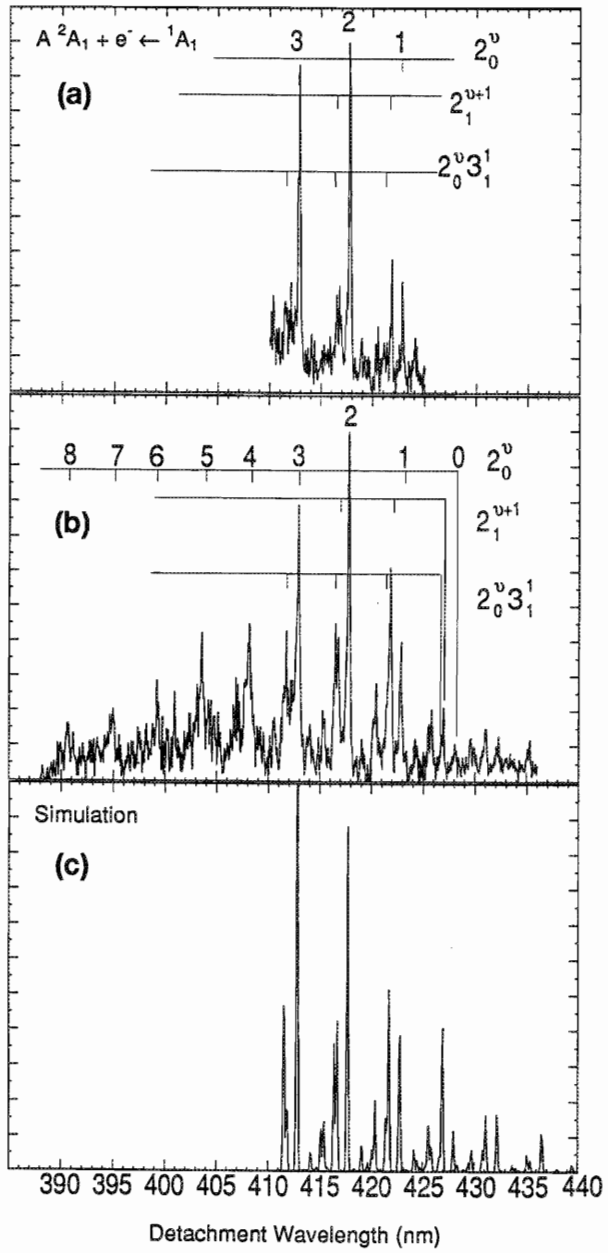

FIG. 6. ZEKE spectrum of InP_2^- to the first excited neutral state (band **A**) obtained under (*a*) liquid-nitrogen-cooled source conditions and (*b*) ambient source conditions. (*c*) The Franck–Condon simulation.

We now consider the modes to which the two observed frequencies correspond. The ω_1 = 204 cm^{-1} frequency is close to the InP diatomic frequency of 257.9 cm^{-1} determined by Weltner [12] by infrared spectroscopy of InP isolated in rare-gas matrices, so it is most likely due to relative In–P motion, namely, the symmetric stretch. The ω_2 = 47 cm^{-1} frequency then must correspond to the bend vibration. The low frequency for this mode suggests it is primarily due to relative In–In motion. In fact, this frequency is considerably lower than the calculated In_2

TABLE 2. Peak positions and assignments for band X in the InP_2^- ZEKE spectrum

Peak position (nm)	Relative energy (cm^{-1})	Assignment
771.35	−78	2_2^2
769.25	−42	2_1^1
766.76	0	Origin; EA = 1.617 eV
759.98	116	2_2^3 , $2_0^1 3_1^1$
757.68	156	2_1^2
755.94	187	2_0^1
749.41	302	$2_0^2 3_1^1$, 2_2^4
746.96	346	2_1^3
745.23	377	2_0^2
741.10	451	$2_1^4 3_1^1$
739.06	489	$2_0^3 3_1^1$
736.59	534	2_1^4
734.50	573	2_0^3
733.3	595	
729.0	675	$2_0^4 3_1^1$
726.3	726	2_1^5
724.4	763	2_0^4
721.6	816	$2_0^5 3_1^1$; $1_0^1 2_1^3$
719.2	862	$2_0^5 3_1^1$; $1_0^1 2_0^2$
716.7	911	2_1^6
714.6	952	2_0^5
711.6	1011	$1_0^1 2_1^4$
709.8	1046	$1_0^1 2_0^3$
707.1	1100	2_1^7
705.1	1140	2_0^6
702.1	1201	$1_0^1 2_1^5$
700.2	1240	$1_0^1 2_0^4$
695.80	1330	2_0^7
690.00	1451	$1_0^1 2_0^5$
686.70	1520	2_0^8
682.10	1619	$1_0^1 2_0^6$
678.11	1705	2_0^9 , $1_0^2 2_0^4$
673.56	1804	$1_0^1 2_0^7$
669.37	1897	2_0^{10} , $1_0^2 2_0^5$
665.07	1994	$1_0^1 2_0^8$
660.94	2088	2_0^{11}
656.97	2179	$1_0^1 2_0^9$
652.65	2281	2_0^{12}
649.0	2366	$1_0^1 2_0^{10}$
645.0	2462	2_0^{13}
641.0	2559	$1_0^1 2_0^{11}$
637.0	2657	2_0^{14}
633.4	2746	$1_0^1 2_0^{12}$
629	2856	2_0^{15}

ground-state frequency, 100 cm^{-1} [20] suggesting very weak bonding between the two indium atoms in In_2P. Weltner also observed an infrared transition at 249.3 cm^{-1}, which was assigned to the ω_3 antisymmetric stretch mode of In_2P. In a triatomic C_{2v} molecule with weak binding between the end atoms, the antisymmetric stretch frequency is typically higher than the symmetric stretch, so our assignment of the ν_1 mode and Weltner's assignment of the ν_3 mode appear consistent.

Although it is straightforward to assign the main progressions and determine neutral vibrational frequencies for the active modes, it is more difficult to determine the anion frequencies and assign the sequence and hot band progressions. To do so, it is useful to simulate the spectrum for an assumed set of anion and neutral frequencies. This is done within the Franck–Condon approximation, where the intensity I of a transition between vibrational levels υ'' and υ' of the anion and neutral, respectively, is assumed proportional to the Franck–Condon factors:

$$I(\upsilon' \leftarrow \upsilon'') \propto \left| \langle \chi'_{vib} \left| \chi''_{vib} \rangle \right| \right|^2 \qquad (2)$$

The vibrational wave functions, χ_{vib}, are taken to be a product of a Morse oscillator wave function corresponding to the symmetric stretch and two harmonic oscillator wave functions corresponding to the symmetric bend and antisymmetric stretch normal modes. The anion and neutral symmetric mode wave functions are displaced from one another along their corresponding normal coordinates until the observed peak intensities are matched. Our simulations assume that the vibrational modes in the anion and neutral are separable and parallel. These are certainly reasonable approximations, since we are not trying to extract detailed geometric displacements from our analysis.

In the simulations shown as the bottom trace in Fig. 3, the following frequencies were used: $\omega_1'' = 295$ cm^{-1}, $\omega_1' = 207$ cm^{-1} ($\omega_1\chi_1' = 3$ cm^{-1}), $T_1 = 150$ K; $\omega_2'' = 100$ cm^{-1}, $\omega_2' = 47$ cm^{-1}, $T_2 = 70$ K; $\omega_3'' = 223$ cm^{-1}, $\omega_3' = 249.3$ cm^{-1} (Weltner's tentative value from matrix work [12]), $T_3 = 140$ K. The simulation matches the experimental peak spacings quite well (the peak indicated with the arrow has not been fit in the simulation). The peak assignments indicated on the combs in Fig. 3 were determined by this simulation, where υ corresponds to υ_2'. Most of the structure observed in the spectrum is attributed to transitions from vibrationally cold anions. The individual peak assignments are listed explicitly in Table 1.

Since there were relatively few intense peaks originating from vibrationally excited anion levels, choosing the anion frequencies for the simulation and assigning the hot band and sequence band structure was not straightforward. The anion symmetric stretch frequency (ω_1'' = 295 cm^{-1}) was chosen such that the hot band positions between 519 and 525 nm could be reasonably matched, treating them as the $2_0^v 1_1^0$ hot band progression. It is not a uniquely determined frequency, as the spectrum could have been fit satisfactorily using 270 or 317 cm^{-1} (i.e., displaced by one-half of a bend quantum) for ω_1''. Overall, however, this is the most reasonable assignment for these transitions. The frequency of 295 cm^{-1} is too high for these transitions to originate from the υ_2'' = 1 anion level, and transitions of the type $2_0^v 3_1^0$ are not allowed because the ν_3 mode is not totally symmetric.

We next consider the progression assigned as the $2_0^v 3_1^1$ sequence band progression. This progression is displaced 27 cm^{-1} to the blue of the 2_0^v progression, indicating that the anion frequency in the mode responsible for this structure is 27 cm^{-1} less than the neutral frequency, so our assignment implies that $\omega_3'' - \omega_3' = -27$ cm^{-1}. Using Weltner's value for ω_3' yields ω_3 = 223 cm^{-1}. This number is uncertain, however, because the origin of the $2_0^v 3_1^1$ progression is difficult to pinpoint.

If, for example, the true origin is 20 cm^{-1} to the red of the 2_0^v progression instead of 27 cm^{-1} to the blue, this would mean that $\omega_3'' - \omega_3' = 20$ cm^{-1} and that $\omega_3'' = 269$ cm^{-1}. We prefer the lower value but acknowledge it may be incorrect.

The alternate assignment of this progression as the 2_1^{v+1} hot band progression was rejected for the following reason. We found that the profile of the 2_0^v progression was best fit assuming a much greater anion ω_2'' frequency than the 47 cm^{-1} neutral frequency. When we attempted to fit the spectrum assuming comparable frequencies, the simulated progression was considerably more extended than the observed spectrum. For example, the normal coordinate displacement could be adjusted until the simulated 2_0^2 peak was the most intense of the 2_0^v progression, as in the spectrum, but the simulated 2_0^1 and 2_0^3 transitions were much more intense relative to the 2_0^2 transition than what was observed. However, using a much greater anion frequency, i.e., a narrower anion bend potential, the anion wave function is more localized, causing it to have good overlap with fewer neutral wave functions. This yields a narrower progression. The anion frequency in the simulation had to be at least 100 cm^{-1} to reproduce the experimental intensity distribution, implying considerably stronger bonding between the indium atoms.

Given this, it seems surprising that there was no obvious hot band structure that we can attribute to ν_2. However, we found that when the anion symmetric bend frequency was chosen to be a near multiple of the neutral frequency, such as 100 cm^{-1}, the simulation would show no distinct sequence or hot bands in ν_2 (except for possibly the peak indicated with the asterisk, which is fit as a 2_1^1 sequence band in the fit presented). The 100 cm^{-1} anion ν_2 frequency we chose for the presented spectrum cannot be considered definitive; the spectral profile could also be fit satisfactorily assuming $\omega_2'' = 150$ cm^{-1}.

Our overall assignments thus indicate that the symmetric stretch and bend frequencies are higher in the anion than the neutral, with the biggest change occurring in the ν_2 mode. If our assignments are correct, they imply considerably stronger bonding between the two indium atoms in the anion as compared to the neutral. In Sect. 5 it will be shown that this is consistent with the expected anion and neutral molecular orbital occupancies.

4.1.2. Approximation of the geometry differences between the anion and neutral

Since we do not know the exact form of the normal coordinates or the geometries for either the anion or the neutral, we cannot quantitatively determine the geometry differences between them. We can, however, obtain an estimate of the change in In—In bond distance between the anion and neutral, assuming the ν_2 mode is primarily an In–In relative motion, which seems likely given the low frequency. The 2_0^v progression was fit using an In diatomic, with a neutral frequency of 47 cm^{-1} and an anion frequency of 100 cm^{-1}, and an absolute bond length difference of approximately 0.2 Å (the In–In distance is presumably smaller in the anion). This is a small change, considering that the calculated In—In bond distance in In_2Sb is 4.6 Å. Assuming an In—P bond distance 0.1 Å greater than the bulk bond distance of 2.54 Å (the In—Sb bond distance in In_2Sb is calculated to be approximately 0.1 Å greater than the bulk bond distance) and a neutral In—In bond distance of 4.6 Å, this corresponds to a bond angle change from 112° in the anion to 120° in the neutral. This is, however, a crude approximation and should be treated with appropriate caution.

TABLE 3. Peak positions and assignments for band **A** in the InP_2^- ZEKE spectrum

Peak position (nm)	Relative energy (cm^{-1})	Assignment
435.21	−386	
432.20	−226	2_1^0
431.00	−161	2_2^1
429.84	−99	2_3^2
429.49	−80	
428.03	0	Origin; $T_e = 1.280$ eV
426.86	64	2_1^1
425.86	119	2_2^2
425.73	126	
425.49	139	
424.32	204	2_3^3
422.79	289	2_0^1
421.74	348	2_1^2
420.42	423	2_2^3
420.14	439	$2_1^2 3_1^1$
419.10	498	2_3^4 ; $2_2^3 3_1^1$; $2_1^2 3_2^2$; etc.
417.71	577	2_0^2
416.72	634	2_1^3
416.37	654	$2_0^2 3_1^1$
415.42	709	2_2^4 ; $2_1^3 3_1^1$; $2_0^2 3_2^2$
414.03	790	2_3^5 '$2_2^4 3_1^1$; etc.
412.80	862	2_0^3
411.62	931	$2_0^3 3_1^1$
410.54	995	2_2^5 ; $2_1^4 3_1^1$; etc.
408.08	1142	2_0^4
403.45	1423	2_0^5
399.15	1690	2_0^6
394.91	1959	2_0^7
390.51	2245	2_0^8

4.2. InP_2^-/InP_2

Based on the discussion at the beginning of this section, we expect InP_2^- and InP_2 to have C_{2v} symmetry. Therefore, we will only discuss the InP_2^- ZEKE spectrum in terms of $C_{2v} \leftarrow C_{2v}$ transitions. Both bands in the InP_2^- spectrum are much more congested and complicated than band **X** in the In_2P^- spectrum, and spectral simulations of both bands **X** and **A** in the InP_2^- spectrum have proven unsatisfactory, since the intensity profiles of both bands appear anomalous. Nonetheless, the simulations have aided in sorting through the numerous sequence bands and combination bands observed in the spectra and will now be discussed in some detail.

4.2.1. Band X vibrational structure and peak assignments

As discussed in Sect. 3, one can extract two vibrational frequencies for the **X** state of neutral InP_2 from the ZEKE spectrum in Fig. 5: $\omega_1' = 478$ cm^{-1} and $\omega_2' = 190$ cm^{-1}. The frequency for the ν_2 mode is comparable to the In–P symmetric stretch frequency in In_2P (204 cm^{-1}) and the diatomic InP frequency

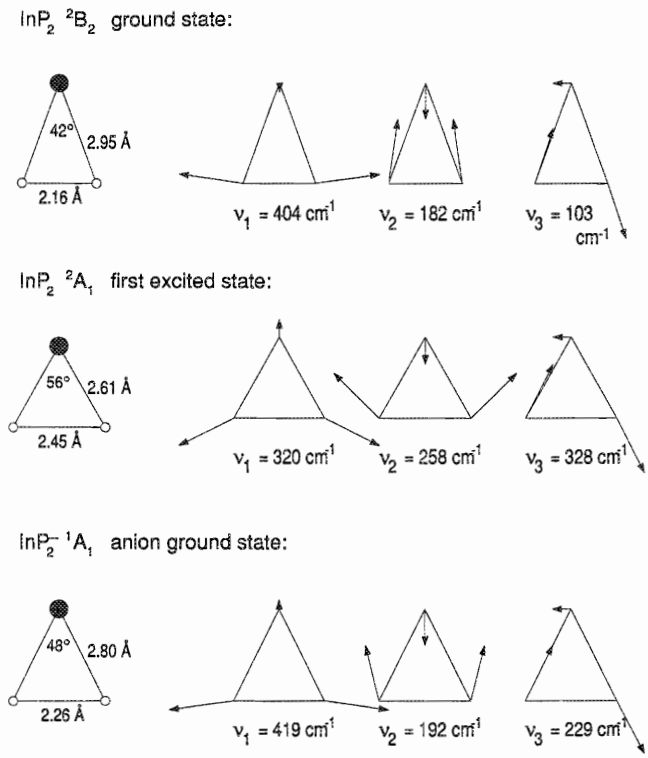

FIG. 7. Geometries and normal coordinates of InP_2/InP_2^- from MP2/LANL1DZ calculations.

(253 cm^{-1}) and is in good agreement with the calculated 182 cm^{-1} ν_2 value for the $^2B_2$ neutral state (Sect. 3.2.). It is therefore reasonable to assign the ν_2 mode to the InP_2 symmetric stretch and to expect this mode to consist primarily of In–P relative motion, as is consistent with the calculated normal coordinate for this mode. The ν_1 frequency, higher than but comparable to the calculated ν_1 frequency, is approximately two thirds of the P_2 triple-bonded ground-state ($^1\Sigma_g^+$) frequency, 780 cm^{-1}, suggesting that this mode consists primarily of P–P relative motion between two doubly bonded phosphorus atoms. The frequencies therefore suggest a bonding scheme in which the indium atom is singly bonded to each P atom, and this costs one bond between the two P atoms. This is also consistent with the calculated geometry for the $^2B_2$ ground neutral state, in which the P—P bond distance, 2.16 Å, is slightly longer than the P_2 ground-state ($^1\Sigma_g^+$) bond distance, 1.89 Å, but is comparable to the bond distance of the P_2 first excited state ($^1\Sigma_u^+$), 2.12 Å.

Band **X** of the InP_2^- ZEKE spectrum was simulated using (2) with the above values for ω_1' and ω_2'; the remaining anion and neutral frequencies are discussed below. The simulation, shown in the bottom panel of Fig. 5, appears to reasonably fit the main features of band **X** in the center panel, namely, the 2_0^v and $1_0^1 2_0^v$ progressions. The simulation also includes the $1_0^2 2_0^v$ progression, not labeled in Fig. 5, which overlaps the higher energy peaks in the 2_0^v progression. The ν_2 mode clearly shows the most activity, suggesting that the biggest geometry change between the anion and neutral is in the In—P bond length.

The simulations also helped identify two hot band progressions, the 2_1^{v+1} and $1_0^1 2_1^{v+1}$ progressions, and a sequence band progression, $2_0^v 3_1^1$ the progression. This assignment of the two hot band progressions yields $\omega_2'' = 227$ cm^{-1} for the anion, which is in qualitative agreement with the calculated value, 192 cm^{-1}. Based on this, the origin of the progression, namely the transition, should appear 227 cm^{-1} to lower photon energy of the 2_0^v origin. However, we found that when we scanned to lower photon energy (under the $N_{2(l)}$-cooled source conditions) the signal-to-noise ratio S/N in this energy region was such that no additional structure was observed. The 2_1^{v+1} assignment is based on the intensity distribution of the 2_1^{v+1} progression, which differs from the main 2_0^v progression in that it peaks earlier (at $v = 3$) and dies off much more rapidly. Such a difference is expected for a hot band because there is a node in the $v_2'' = 1$ wave function where the $v_2'' = 0$ wave function is a maximum. Hence the Franck–Condon factors for the two anion levels are quite different. In principle, the intensity distribution in an extended hot band progression should be bimodal. This is seen in the simulated progressions, in which the intensity distribution peaks on both sides of the minimum at $v_2' = 5$. However, the experimental progression does not rise again at higher v_2'; this may be related to the whole progression dying out at lower energy than is observed in the PES (see Fig. 4), or to the various approximations in our Franck–Condon analysis.

The remaining sequence band progression was assigned to the $2_0^v 3_1^1$ progression rather than the $1_0^1 2_0^v$ progression based on the results of the ab initio frequency calculations (Sect. 3.2.). The calculations predict that the anion ν_3 frequency is on the order of 200 cm^{-1} lower than the ν_1 frequency. This means that the anion $v_3 = 1$ level should be more populated than the $v_1 = 1$ level, so the sequence band in the ν_3 mode should be more intense. Since the $2_0^v 3_1^1$ progression is displaced 75 cm^{-1} to the red of the 2_0^v progression, we have $\omega_3'' - \omega_3' = 75$ cm^{-1}, which is in qualitative agreement with the calculated difference, 126 cm^{-1}.

4.2.2. Band A vibrational structure and peak assignments

By comparing the spectra of band **A** obtained under different source conditions (top and middle panels of Fig. 6), there appears to be only one progression originating from the anion ground state with a peak spacing of 287 cm^{-1}. The neutral vibrational mode associated with this progression cannot be determined based on comparison with the ab initio frequencies calculated for the $^2A_1$ excited state, as 287 cm^{-1} is equally close to both of the calculated symmetric frequencies (see Fig. 7). However, the relative geometries calculated for the anion and the $^2A_1$ neutral state suggest that the ν_2 bend, in which the P—P bond elongates while the In—P bond contracts (and vice versa), should be more active than the ν_1 stretch, in which both bonds elongate (or contract). Therefore, the progression has been assigned to 2_0^v transitions, with $\omega_2' = 287$ cm^{-1}. It is also interesting to note from Fig. 7 that in the ground state, ν_1 is primarily a P–P stretch and ν_2 an In–P stretch, whereas in the $^2A_1$ state, ν_1 and ν_2 are better described as the symmetric stretch and bend, respectively, and both modes involve the relative motion of all three atoms.

The Franck–Condon simulation in Fig. 6 shows that one can account for most of the structure in addition to the main progression with two more progressions, the 2_1^{v+1} hot band progression and the $2_0^v 3_1^1$ sequence band. Explicit peak assignments are listed in Table 3. The 2_1^{v+1} progression was fit assuming $\omega_2'' = 227$ cm^{-1} in the anion, the same value found for the 2_1^{v+1} progression in band **X**. As in band **X**, the intensity distribution peaks earlier for the 2_1^{v+1} progression than for the 2_0^v progression. The $2_0^v 3_1^1$ sequence bands were so assigned by the same arguments given in the previous section, namely that ab initio calculations predict $\omega_1'' > \omega_3''$ for the anion, in which case $\omega_3'' - \omega_3' = -75$ cm^{-1} (the calculated difference is –99 cm^{-1}).

Note this is opposite in sign to $\omega_3'' - \omega_3'$ in band **X**. In the simulation, the remaining, lower-intensity peaks were fit by the $2_0^v 3_2^2$, $2_1^{v+1} 3_1^1$ and 2_2^{v+2} transitions.

The 287 cm^{-1} ν_2 frequency for this excited state is substantially higher than the 190 cm^{-1} frequency observed for the ground state, suggesting that there is more phosphorus relative motion involved in the excited state ν_2 mode. Based on this, we can infer that the P–P bonding is weaker and the In–P bonding is stronger in this first excited state. This is supported by the calculated geometries for the two neutral states. The 227 cm^{-1} anion ν_2 frequency fits in nicely as having intermediate bonding properties between the two neutral states, suggestive of the orbital occupancies the anion has in common with the two neutral states. The molecular orbital configurations for the anion and two neutral states will be discussed in the following section.

A notable feature of band **A** is that the peaks in the main progression broaden somewhat for $v_2' \geq 3$, suggesting there is a perturbation affecting the neutral state that turns on between peaks 2_0^2 and 2_0^3. This perturbation is clearly different in nature than the intensity fall-off compared to the photoelectron spectrum that occurs in band **X**, in which the higher-energy peaks maintained narrow peak widths, and the signal-to-noise ratio remained quite good. One possibility is that the peak broadening is from dissociation to In + P_2. The dissociation energy for $InSb_2 \rightarrow In + Sb_2$ is calculated to be only 1.3 eV [7]. Since T_e for the InP_2 first excited state is 1.280 eV, it is certainly feasible that at least part of band **A** lies above the dissociation continuum, thereby causing the broadening of peaks at the higher energy end of the band. The ν_2 normal coordinate would appear to facilitate dissociation; a displacement negative of the coordinate shown in Fig. 7 gives closer phosphorus atoms combined with a longer In–P distance. Assuming that dissociation is occurring, from the position of peak 2_0^3, which is slightly wider than 2_0^2, the dissociation energy of InP_2 lies between 1.352 and 1.386 eV.

Another explanation for the peak broadening is suggested by Balasubramanian's [7] calculations on $InSb_2$, which predict that the potential energy curves for the first excited ($^2A_1$) state and ground $^2B_2$ state cross just above the $^2A_1$ minimum. These states interact strongly via spin-orbit coupling. If there is a similar curve crossing in InP_2, one might expect the energy levels of the excited state that lie above the intersection point to be badly perturbed, possibly leading to the broadening seen in band **A** of our spectrum.

5. Discussion

5.1. In_2P^-/In_2P electronic state assignments

From the vibrational analysis of the In_2P^- ZEKE spectrum, we concluded that the anion bend frequency is higher than the neutral bend frequency, implying that the In—In bond is stronger in the anion than the neutral. Moreover, given the low frequency of the bend mode in In_2P ($\omega_2' = 47$ cm^{-1}), the 2_0^v progressions in the ZEKE spectrum are quite short, indicating a relatively small displacement along the ν_2 normal coordinate between the anion and neutral. One would like to understand these results in terms of the molecular orbital configurations of In_2P and In_2P^-. Although no ab initio calculations have been performed on either species, Balasubramanian has determined the dominant molecular orbital configurations for the isovalent neutral In_2Sb and Ga_2As [7], and these serve as a starting point for our discussion.

The ground electronic states of In_2Sb and Ga_2As were calculated to have C_{2v} geometries with a $^2B_1$ electronic character from the following valence orbital occupancy:

$$1a_1^2 2a_1^2 1b_2^2 2b_2^2 3a_1^2 1b_1^1 (4a_1^0) \quad (3)$$

Qualitative pictures of these orbitals are shown in Fig. 8; these are adapted from the description by Balasubramanian [7] and the pictures of Meier et al. [9] Note that the half-filled $1b_1$ orbital is an out-of-plane orbital with most of its amplitude on the two end atoms. Although vibrational frequencies were not determined for In_2Sb or Ga_2As, potential energy curves were calculated for the ground and low-lying excited states as a function of bend angle [7]. The equilibrium bend angles for In_2Sb and Ga_2As were found to be 104° and 109.5°, respectively, and both species were calculated to have very broad bend potentials, with fairly weak bonding between the two group III atoms. This is qualitatively consistent with the low bending frequency seen for the In_2P ground state, and it seems reasonable that the ground state of In_2P is also a $^2B_1$ state with the valence configuration of (3).

The anion electronic orbital occupancy may be determined by adding an electron either to the $1b_1$ orbital, resulting in a $^1A_1$ state, or possibly the $4a_1$ orbital, giving a $^3B_1$ state. Both of these orbitals are bonding between the two end atoms, so in either case one would expect the anion to be more bent and to have a higher bend frequency than the neutral. The $1b_1$ orbital should be less strongly bonding between the In atoms than the $4a_1$ orbital which, given the relatively small geometry change suggested by the short 2_0^v progression, may favor the $^1A_1$ state for the anion. This is consistent with Balasubramanian's calculations on the excited states of neutral In_2Sb which predict that states formed by promoting an electron from the $3a_1$ or $2b_2$ orbitals to the $1b_1$ orbital are lower in energy than the quartet states formed by promoting the same electrons to the $4a_1$ orbital. However, that the anion ν_2 frequency is substantially greater than the neutral might suggest the $^3B_1$ state. We hesitate to make a definite anion state assignment lacking more definitive anion frequencies, especially for the ν_2 mode.

5.1.1. Band A (or lack thereof)

Given that In_2P^- is more bent than the neutral ground state, and that in the In_2P^- photoelectron spectrum the widths of bands **X** and **A** are similar, the most likely candidate for the neutral excited state responsible for band **A** is the $^2B_2$ state; the $^2B_2$ state in In_2Sb is predicted to have a bend angle of 80° versus 104° for the $^2B_1$ ground state [7]. A low-lying linear ($^2\Pi_u$) state of In_2Sb is also predicted, but the photodetachment transition to this state should be much more extended than band **A** owing to the large change in bend angle between anion and neutral, so it is a less likely candidate for the upper state in band **A**.

It still remains unexplained why band **A** is not present in the ZEKE spectrum. The selection rules for negative ion threshold photodetachment are more restrictive than for PES, due to the Wigner threshold law. For atomic systems, this dictates that the detachment cross section near threshold goes as [21]

$$\sigma \propto \sigma_0 (E_{h\nu} - E_{\text{threshold}})^{l+1/2} \quad (4)$$

where $(E_{h\nu} - E_{\text{threshold}})$ is the energy above threshold (i.e., the kinetic energy of the detached electron), and l is the angular momentum of the ejected electron. The result is that only electrons with $l = 0$ (s wave) have a sharply rising cross section near threshold, a necessary condition to observe a ZEKE transition. This has been applied to polyatomic anions by Reed et al. [22], who point out that only electrons from MO's (molecular orbitals) with the same transformation properties as the x, y, or z body-fixed coordinates can undergo s-wave detachment. In a C_{2v} molecule, all orbitals except those with a_2 symmetry can

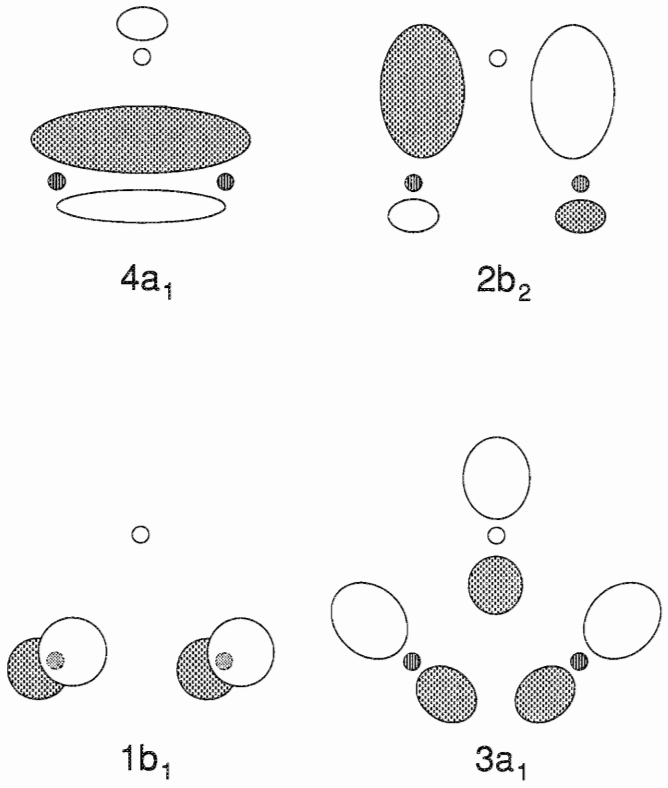

FIG. 8. Qualitative representations of the high-lying molecular orbitals of In_2P and InP_2.

detach with $l = 0$. Hence, from the discussion in the previous section, *s*-wave detachment is allowed for any one-electron photodetachment transition from a $^1A_1$ anion involving the valence orbitals. This would be true if the anion were a $^3B_1$ state as well, see (3). In either case one would expect band **A** in the In_2P^- photoelectron spectrum to appear in the ZEKE spectrum as well.

However, as was pointed out by Reed et al. [22] the selection rule for *s*-wave detachment is a necessary but not sufficient condition for a sharply rising cross section near threshold. Indeed, our work on Si_3^- [4] showed that several bands in the photoelectron spectrum in which *s*-wave detachment was allowed did not appear in the ZEKE spectrum. An important factor here is how much the orbital from which detachment occurs resembles an atomic *p*-orbital. Of all the orbitals in Fig. 8, the $1b_1$ appears to have the most atomic *p*-character, so removal of an electron from this orbital should result in a strong ZEKE signal. In fact, band **X** gives the most intense ZEKE signal for any molecular anion we have studied thus far, consistent with its assignment as a $^2B_1 \leftarrow {}^1A_1$ (neutral ← anion) transition. However, it is far from clear that the $1b_2$ orbital deviates from an atomic *p*-orbital to a sufficient extent that we could not observe ZEKE signal for the transition to the $^2B_2$ excited state. The determination of conditions sufficient for strong *s*-wave photodetachment is an interesting and important question for future study as it determines the range of applicablity of anion ZEKE spectroscopy.

5.2. InP_2^-/InP_2 electronic states

The experimental anion and neutral vibrational frequencies for InP_2 and InP_2^- are, in general, consistent with the calculated properties of the anion and two neutral states shown in Fig. 7, supporting our identification of the experimentally observed states with the three calculated states. In this section, we compare the properties of these states to the calculated properties of the analogous ground $^2B_2$ and excited $^2A_1$ states of $GaAs_2$ and $InSb_2$ [7, 9] as well as the ground $^1A_1$ state of $GaAs_2^-$ [9]. The calculations on these InP_2 analogs were considerably more sophisticated and complete than our calculations on In_2P and In_2P^- (although no vibrational frequencies were determined in the earlier studies), so they provide a useful framework for understanding the chemical bonding in In_2P and In_2P^-.

The ground $^2B_2$ electronic state orbital occupancy of InP_2, $GaAs_2$, and $InSb_2$ is

$$1a_1^2 2a_1^2 1b_2^2 3a_1^2 1b_1^2 4a_1^2 3b_2^1 (1a_2^0) \qquad (5)$$

Two close-lying neutral states, the $^2A_1$ and $^2B_1$ states (with calculated T_e of 0.67 and 1.38 eV, respectively, for $InSb_2$) are formed by promoting a $4a_1$ and a $1b_1$ electron, respectively, into the $2b_2$ orbital. The ground and first excited electronic orbital occupancies here are those used in the ab initio geometry and frequency calculations described in Sect. 3.2. for InP_2 (Fig. 7). The anion $^1A_1$ ground state is formed by adding an electron to the $2b_2$ orbital of the $^2B_2$ state. The $^3B_1$ state with unpaired electrons in both the $2b_2$ and $1a_2$ orbitals was found to lie only 0.5 eV higher in energy for $GaAs_2^-$ [9].

Figure 7 shows that, compared to the InP_2 $^2B_2$ ground state, the P—P bond distance is longer in the anion and the In—P bond distance is shorter. This reflects the effect of the additional electron in the $2b_2$ orbital, which is antibonding between the two phosphorus atoms but bonding between the indium and phosphorus atoms (see Fig. 8). Figure 7 shows that the $^2A_1$ neutral state has a wider bond angle and shorter In–P distance than the neutral ground state; this is consistent with having two electrons in the $2b_2$ orbital but only one in the strongly P–P bonding $4a_1$ orbital.

Our calculated energy separation for the $^2B_2$ and $^2A_1$ states of In_2P is 1.139 eV, which is quite close to the observed energy, 1.280 eV. This is approximately twice the calculated term energy for the analogous $GaAs_2$ and $InSb_2$ $^2A_1$ states [7, 9]. The large difference can be understood by considering how the $2b_2$ and $4a_1$ orbitals correlate to the P_2 diatomic and In atomic orbitals. The $4a_1$ orbital is formed from the $2\pi_u + 5p$ orbitals, while the $2b_2$ orbital correlates with the $2\pi_g + 5p$ orbitals. The energy difference between the $2\pi_u$ and $2\pi_g$ orbitals in P_2 is greater than for As_2 or Sb_2 [23],[3] causing the $4a_1 - 2b_2$ splitting to be greater in InP_2 than for $GaAs_2$ or $InSb_2$.

An interesting issue in these clusters is the degree of covalent vs. ionic bonding. In bulk InP, the bonding is largely ionic, with excess negative charge on the P atoms. However, there are no P—P bonds in crystalline InP, whereas there is strong P–P bonding in InP_2, suggesting a covalent bonding picture. On the other hand, Balasubramanian calculated the dipole moments associated with the various electronic states and structural isomers of the GaAs and InSb mixed triatomics [7]. Dipoles of 1.22 and 1.64 D were determined for the $^2B_2$ C_{2v} states of $GaAs_2$ and $InSb_2$, respectively. As the difference in electronegativity between In and P is greater than for Ga and As, or In and Sb, it would follow that the dipole of the $^2B_2$ state of InP_2 is greater than for $GaAs_2$ or $InSb_2$. This is confirmed by our ab initio calculations, which gave 3.6 D for the $^2B_2$ state and 3.55 D for

[3]This reference indicates that the dissociation energies of the As_2 and Sb_2 ground $^1\Sigma_g^+$ state are lower than that of the P_2 $^1\Sigma_g^+$ state.

the $^2A_1$ state. Therefore, despite the substantial amount of covalent bonding between the two phosphorus atoms in this molecule, the dipole suggests that there is still ionic character along the In—P bond. It is not suprising that the two partially negative phosphorus moieties are so strongly bound in the ground InP_2 state, as P_2^- has been found to be strongly bound (D_0 = 4.88 eV) with a bond distance of 1.98 Å [24], which is only 0.09 Å longer than the neutral bond distance.

6. Conclusions

The ZEKE spectra of the two InP triatomics have shown that these very small clusters are remarkably complex. The two triatomics we have investigated are very different from one another. Although both have C_{2v} geometries, the In_2P ground state has very weak In–In bonding, an obtuse bond angle, and a very broad potential, in contrast to the InP_2 ground state, which has very strong P–P bonding, an acute bond angle, and a fairly steep bend potential. The geometry differences between the anions and neutrals seem to be much more dramatic for InP_2 than for In_2P.

The In_2P^- ZEKE spectrum shows progressions in both the 47 cm^{-1} symmetric bend (ν_2) and the 204 cm^{-1} symmetric stretch (ν_1) of the C_{2v}, $^2B_1$ neutral ground state. From the profile of the progressions and the limited sequence and hot band structure, we can infer that all modes of the anion have higher frequencies than the neutral, which is consistent with the anion having the extra electron in the $1b_1$ orbital. The transition to what we believe is the $^2B_2$ state observed in the previously obtained PES is not observed in the ZEKE spectrum.

Based on trends in ν_2 frequencies between the two neutral states and the anion, the ground state of InP_2 is determined to have a $^2B_2$ and a $^2A_1$ first excited electronic state at 1.280 eV above the ground state. This is analogous with the calculated ground and first excited states for $InSb_2$ and $GaAs_2$ where the $^2B_2$ ground state and the $^2A_1$ first excited state are separated by less than 1 eV. The anion ground state appears to be the $^1A_1$ state. The $^2B_2$ ground state of InP_2 exhibits much stronger P–P bonding and weaker In–P bonding relative to the first excited $^2A_1$ state, and the anion has bonding properties intermediate between the two neutral states. It is clear from our analysis of the spectra, which was supported by our ab initio calculations, that although the electronic states of this small cluster are fairly close-lying, the vibrational properties are dramatically influenced by simply shifting an electron from the $4a_1$ orbital to the $2b_2$ orbital.

Acknowledgments

This work was supported under National Science Foundation grant DMR-9201159. Thanks go to Don Arnold for help with calculations and to Mary Mandich for generously supplying us with our first InP rod.

1. J. Faist, F. Capasso, D.L. Sivco, C. Sirtori, A.L. Hutchinson, and A.Y. Cho. Science (Washington, D.C.), **264**, 553 (1994).
2. E.C. Honea, A. Ogura, C.A. Murray, K. Raghavachari, W.D. Sprenger, M.F. Jarrold, and W.L. Brown. Nature (London), **366**, 42 (1993).
3. T.N. Kitsopoulos, C.J. Chick, A. Weaver, and D.M. Neumark. J. Chem. Phys. **93**, 6108 (1990).
4. C.C. Arnold and D.M. Neumark. J. Chem. Phys. **99**, 3353 (1993).
5. C.C. Arnold and D.M. Neumark. J. Chem. Phys. **100**, 1797 (1994).
6. R.O. Jones. Phys. Rev. A, **32**, 2589 (1985); K. Raghavachari and V. Logovinsky. Phys. Rev. Lett. **55**, 26 (1985); G. Pacchioni and J. Koutecky. J. Chem. Phys. **84**, 3301 (1986); A. Slanina. Chem. Phys. Lett. **131**, 420 (1986); K. Balasubramanian. Chem. Phys. Lett. **135**, 283 (1987); C.M. Rohlfing and K. Raghavachari. Chem. Phys. Lett. **167**, 559 (1990); R. Fournier, S.B. Sinnott, and A. DePristo. J. Chem. Phys. **97**, 4149 (1992).
7. K. Balasubramanian. J. Chem. Phys. **87**, 3518 (1987); K.K. Das and K. Balasubramanian. J. Chem. Phys. **94**, 6620 (1991).
8. M.A. Al-Laham, G.W. Trucks, and K. Raghavachari. J. Chem. Phys. **96**, 1137 (1992); M.A. Al-Laham and K. Raghavachari, Chem. Phys. Lett. **187**, 13 (1991); K. Raghavachari. J. Chem. Phys. **101**, 5406 (1994).
9. U. Meier, S.D. Peyerimhoff, and F. Grein. Chem. Phys. **150**, 331 (1991).
10. L. Lou, L. Wang, L.P.F. Chibante, R.T. Laaksonen, P. Nordlander, and R.E. Smalley. J. Chem. Phys. **94**, 8015 (1991); L. Lou, P. Nordlander, and R.E. Smalley. J. Chem. Phys. **97**, 1858 (1992).
11. R.M. Graves and G.E. Scuseria. J. Chem. Phys. **95**, 6602 (1991).
12. S. Li, R.J. Van Zee, and W. Weltner, Jr. J. Phys. Chem. **98**, 2275 (1994).
13. K.D. Kolenbrander and M.L. Mandich. J. Chem. Phys. **92**, 4759 (1990). Phys. Rev. Lett. **65**, 2169 (1990); K.-D. Rinnen, K.D. Kolenbrander, A.M. DeSantolo, and M.L. Mandich. J. Chem. Phys. **96**, 4088 (1992).
14. T.N. Kitsopoulos, C.J. Chick, Y. Zhao, and D.M. Neumark. J. Chem. Phys. **95**, 5479 (1991).
15. C.C. Arnold, Y. Zhao, T.N. Kitsopoulos, and D.M. Neumark. J. Chem. Phys. **97**, 6121 (1992).
16. T.N. Kitsopoulos, I.M. Waller, J.G. Loeser, and D.M. Neumark, Chem. Phys. Lett. **159**, 300 (1989); C.C. Arnold, Y. Zhao, T.N. Kitsopoulos, and D.M. Neumark. J. Chem. Phys. **97**, 6121 (1992).
17. T.G. Dietz, M.A. Duncan, D.E. Powers, and R.E. Smalley. J. Chem. Phys. **74**, 6511 (1981).
18. K. Müller-Dethlefs, M. Sander, and E.W. Schlag, Z. Naturforsch. Teil A, **39**, 1089 (1984); Chem. Phys. Lett. **12**, 291 (1984); K. Müller-Dethlefs and E.W. Schlag. Annu. Rev. Phys. Chem. **42**, 109 (1991).
19. M.J. Frisch, G.W. Trucks, M. Head-Gordon et al. Gaussian 92, revision C. Gaussian, Inc., Pittsburg, Pa. 1992.
20. K. Balasubramanian and J. Q. Li. J. Chem. Phys. **88**, 4979 (1988).
21. E.P. Wigner. Phys. Rev. **73**, 1002 (1948).
22. K.J. Reed, A.H. Zimmerman, H.C. Andersen, and J.I. Brauman. J. Chem. Phys. **64**, 1368 (1976).
23. G. Herzberg. Molecular spectra and molecular structure, Vol. I. Spectra of diatomic molecules. Robert E. Krieger Publishing Company, Malabar, Fla. 1989. pp. 504, 561, and 566.
24. J.T. Snodgrass, J.V. Coe, C.B. Freidhoff, K.M. McHugh, and K.H. Bowen. Chem. Phys. Lett. **122**, 352 (1985).